Quantum Monte Carlo Simulation of the Chiral Heisenberg Gross-Neveu-Yukawa Phase Transition with a Single Dirac Cone

Thomas C. Lang[*] and Andreas M. Läuchli

Institute for Theoretical Physics, University of Innsbruck, 6020 Innsbruck, Austria

We present quantum Monte Carlo simulations for the chiral Heisenberg Gross-Neveu-Yukawa quantum phase transition of relativistic fermions with $N = 4$ Dirac spinor components subject to a repulsive, local four fermion interaction in $(2 + 1)$D. Here we employ a two-dimensional lattice Hamiltonian with a single, spin-degenerate Dirac cone, which exactly reproduces a linear energy-momentum relation for all finite size lattice momenta in the absence of interactions. This allows us to significantly reduce finite size corrections compared to the widely studied honeycomb and π-flux lattices. A Hubbard term dynamically generates a mass beyond a critical coupling of $U_c = 6.76(1)$ as the system acquires antiferromagnetic order and SU(2) spin rotational symmetry is spontaneously broken. At the quantum phase transition, we extract a self-consistent set of critical exponents $\nu = 0.98(1)$, $\eta_\phi = 0.53(1)$, $\eta_\psi = 0.18(1)$, and $\beta = 0.75(1)$. We provide evidence for the continuous degradation of the quasiparticle weight of the fermionic excitations as the critical point is approached from the semimetallic phase. Finally, we study the effective "speed of light" of the low-energy relativistic description, which depends on the interaction U, but is expected to be regular across the quantum phase transition. We illustrate that the strongly coupled bosonic and fermionic excitations share a common velocity at the critical point.

Right at the interface between bosonic spin and fermionic physics lies the Gross-Neveu-Yukawa (GNY) field theory, which is believed to capture the complex interplay of bosonic and fermionic (quantum) critical fluctuations giving rise to a large set of universal critical exponents [1,2]. The GNY Lagrangian describes relativistic fermions, which interact with a multicomponent bosonic field. For sufficiently strong interactions, the system undergoes a phase transition from a semimetal of massless Dirac fermions to a symmetry broken phase with massive fermionic excitations, in which the order is captured by a $\mathbb{Z}_2$, O(N), or SU(N) symmetric order parameter. The GNY universality class comprises the critical properties of these phase transitions, based not only on the symmetry of the order parameter alone, but it must include the symmetry (degeneracy) of the fermions involved and as such cannot be described within the Landau paradigm of phase transitions. In recent years it has become evident that this physics of relativistic fermions is far from confined to high-energy physics, but manifests in many two- and three-dimensional condensed matter systems [3–7], most prominently among them the carbon allotrope graphene [8] and magic angle twisted bilayer graphene [9–14].

A large number of models in condensed matter physics, which describe the dynamical generation of a gap in interacting Dirac fermions, are widely believed to share the same universal properties at criticality as described by the GNY field theory. The correspondence between the condensed matter models and the GNY field theory can be shown explicitly at low energies [15,16]. Where the chiral

Ising ($\mathbb{Z}_2$) GNY transition [17–30] and the chiral-XY [O(2) or U(1)] GNY transition [17–19,30–43] have been investigated extensively, far fewer results exist for the much more challenging chiral Heisenberg [O(3) or SU(2)] GNY transition in $(2 + 1)$D [15,17,30,44–50], which we focus on in this Letter.

The issue shared among all the investigations is the apparent disparity between the estimates for the critical exponents, not only between complementary methods, but even within different Monte Carlo simulations. The latter could be attributed to the fact that only a small region of the Brillouin zone (BZ) of common lattices, such as the honeycomb lattice and π flux (staggered fermions), actually displays relativistic behavior at low energies [cf., Figs. 1(d)–(f)], and large finite size lattices are required in order to obtain a sufficiently high momentum resolution at low energies to guarantee asymptotic scaling at criticality.

In this Letter, we set out to minimize the finite size effects by implementing a single Dirac cone on the lattice, which allows us to maximize the portion with a relativistic dispersion in the BZ. In addition, rather than distributing the fermion species across different momenta, such as in the implementation of staggered fermions (i.e., the honeycomb or π-flux lattice), or reducing the BZ to patches in momentum space [51], a single Dirac cone is the closest representation of the continuum Dirac operator [52–56]. Furthermore, a single spin-degenerate ($N_f = 2$) Dirac cone constitutes the smallest possible number of fermions
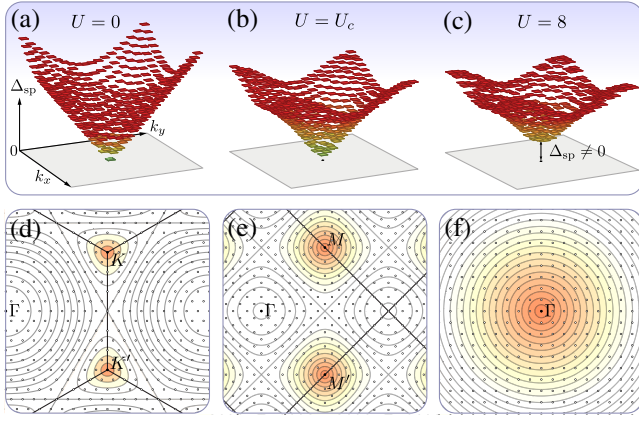
FIG. 1. The momentum resolved single-particle gap from QMC simulations (a) in the chiral limit (b) at the critical point, and (c) in the massive phase in the first Brillouin zone for an $L = 19$ system. The dispersion illustrates the interaction induced spontaneous mass generation for sufficiently strong interactions and the renormalization of the bandwidth across the quantum phase transition. The finite size momentum resolution for an $L = 18$ (d) honeycomb lattice (e) π-flux lattice (staggered fermions), and for (f) SLAC fermions superimposed on the lines of constant energy in the Brillouin zone.

species $N = 2N_f = 4$ or components of the Dirac spinor representation, for which an SU(2) symmetric order parameter can be formulated on a lattice. As such, our investigation provides a benchmark for complementary approaches such as ϵ and $1/N$ expansions, where for small fermion species numbers their estimates for the critical exponents vary the most.

Model and Hamiltonian.—Here we consider a Hamiltonian formulation of relativistic massless fermions with a perfect Dirac cone in energy-momentum space in $(2 + 1)$D. For each fermion flavor $\sigma \in \{1, ..., N_f\}$ the free Hamiltonian for a single Dirac cone on a square lattice with the primitive vectors in the x and y directions and unit lattice constant reads

$$H_{t\sigma} = -v_F^0 \sum_{i=1}^{L^2} \left[i \sum_{x=-L/2}^{L/2} t(x)(a_{i\sigma}^\dagger b_{i+x,\sigma} - b_{i+x,\sigma}^\dagger a_{i\sigma}) \right.$$

$$\left. + \sum_{y=-L/2}^{L/2} t(y)(a_{i\sigma}^\dagger b_{i+y,\sigma} + b_{i+y,\sigma}^\dagger a_{i\sigma}) \right]. \quad (1)$$

Here $a_{i\sigma}^\dagger$ ($b_{i\sigma}^\dagger$) creates an electron with flavor σ in an orbital a (b) of unit cell i, while $i + x$ denotes the unit cell in the x direction at a distance $|x|$. The discrete inverse Fourier transform of the Dirac operator yields the finite size hopping amplitudes $t(r) = (-1)^r \pi/[L \sin(r\pi/L)]$, $r \neq 0$, which in the thermodynamic limit (TDL) $L \to \infty$ implies that the hopping amplitude decays as $t(r) = (-1)^r/r$. The corresponding single-particle spectrum is given by $\varepsilon_\pm(\mathbf{k}) = \pm v_F^0|\mathbf{k}|$ with a $2N_f$-fold degeneracy at $\mathbf{k} = (0, 0)$. In the following we choose the Fermi velocity

$v_F^0 = 1$ as a unit of energy. This setup may be interpreted as a square lattice bilayer with $2L^2$ sites with bipartite interlayer hopping. The lattice derivative in Eq. (1) is the Hamiltonian formulation of SLAC fermions [57]. While SLAC fermions have been shown to be problematic in gauge theories [58], they have been successful in simulations of supersymmetric Yukawa, Wess-Zumino, and Thirring models [40,58–63]. A variation, which corresponds to spinless fermions, has recently been used in Ref. [38] to produce highly accurate results when compared against exactly known critical exponents. SLAC fermions avoid the Nielsen-Ninomiya theorem [64–66] by violating locality on finite size lattices. Locality of the Dirac operator is recovered in the infinite volume limit for most of the BZ, while potentially problematic properties are confined to the singular boundaries of the system [67]. We thus monitor the single-particle excitations, in particular, close to the boundary of the BZ for potentially interfering low-energy modes.

In order to dynamically gap out the chiral fermions and to drive the system through a quantum phase transition, we augment the free Hamiltonian with a local Hubbard-type repulsion $H = \sum_{\sigma=1,2} H_{t\sigma} + (U/2) \sum_{i,c} (n_{i,c} - 1)^2$, where $n_{i,c} = \sum_{\sigma=1,2} c_{i\sigma}^\dagger c_{i\sigma}$ is the local density electrons in orbital $c \in \{a, b\}$. At strong coupling $U \gg v_F^0$ and half filling, the Hamiltonian reduces to a bilayer Heisenberg model with antiferromagnetic Heisenberg interactions only between the layers. The anticipated Dirac semimetal to antiferromagnet (AFM) quantum phase transition is expected to be in the $N = 4$ chiral Heisenberg GNY universality class.

Finally, the Hamiltonian $H_{t\sigma}$ is represented by a Hermitian differentiation matrix and the Hubbard interaction can be decoupled at the cost of introducing a discrete auxiliary field via the Hubbard Stratonovich decomposition, which allows us to perform large-scale, sign-problem-free auxiliary-field quantum Monte Carlo (QMC) simulations at zero temperature [26,68–71].

QMC simulation results.—We track the emergence of long-range AFM order by measuring the spin structure factor $S_{\text{AFM}}(\mathbf{k}) \equiv \sum_\mathbf{r} e^{i\mathbf{k}\cdot\mathbf{r}} \langle \mathbf{S}(\mathbf{r}) \cdot \mathbf{S}(\mathbf{0}) \rangle / L^2$, where $\mathbf{S}(\mathbf{r}) = \mathbf{S}_{\mathbf{r}a} - \mathbf{S}_{\mathbf{r}b}$ is the unit cell AFM order parameter with the spin $\mathbf{S}_{\mathbf{r}a} = \frac{1}{2} a_{\mathbf{r}\alpha}^\dagger \boldsymbol{\sigma}_{\alpha\beta} a_{\mathbf{r}\beta}$ at position $\mathbf{r}$, orbital a, and $\boldsymbol{\sigma}$ denotes the vector of the three Pauli matrices. The evolution of the squared finite size magnetization $m^2 = S_{\text{AFM}}(\mathbf{0})/L^2$ is presented in the Supplemental Material [72]. The critical point beyond which the fermions acquire mass can be precisely determined with the help of the RG invariant correlation ratio $R_{m^2}^{(n_1,n_2)} = 1 - S_{\text{AFM}}(\mathbf{Q} + n_1\mathbf{b}_1 + n_2\mathbf{b}_2)/S_{\text{AFM}}(\mathbf{Q})$, where $\mathbf{b}_1$ and $\mathbf{b}_2$ denote the reciprocal lattice vectors [74,75]. R_{m^2} intersects for different L at the critical coupling point and at a universal but geometry-dependent value $R_{m^2}^*$. We opt for $R_{m^2}^{(1,1)}$ with the least drift of the finite size crossing points shown in Fig. 2(a) (cf., Supplemental Material [72]) and fit the data with the finite size scaling (FSS) ansatz $R_{m^2}(u, L) = f_0^R(uL^{1/\nu}) + L^{-\omega} f_1^R(uL^{1/\nu})$, where
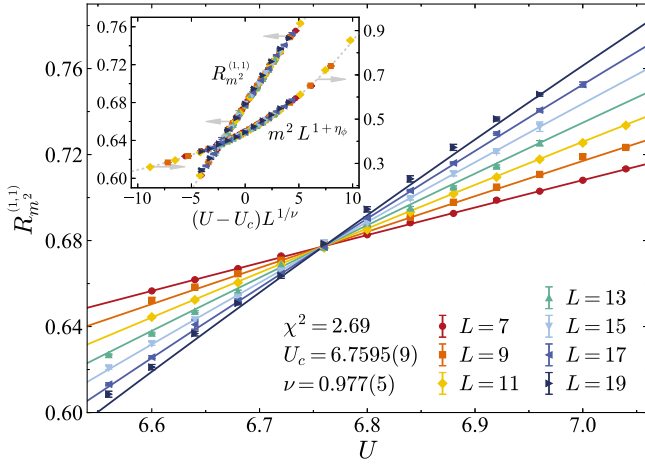
FIG. 2. The correlation ratio close to the critical point from which we extract the critical exponent ν from a fit to the data. (Inset) Data collapse of the correlation ratio (left scale) and the squared magnetization (right scale) using the critical exponents ν and η_ϕ extracted from the data in the main panel and Fig. 3, respectively. Dotted lines indicate the scaling functions.
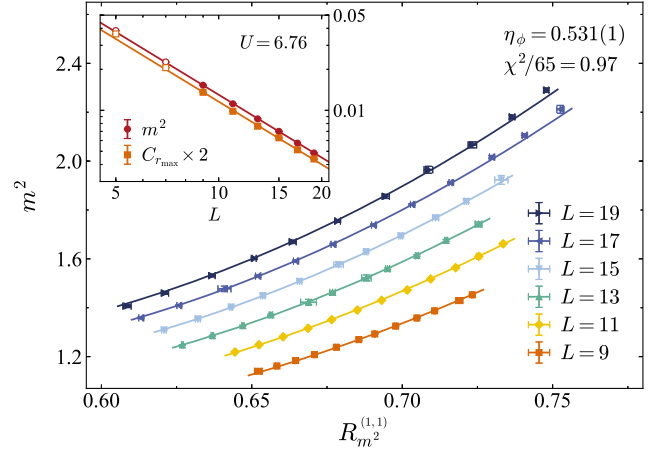

FIG. 3. Fit of the finite size scaling ansatz to the squared magnetization of the single-particle correlation function in order to extract the bosonic and fermionic anomalous dimensions η_ϕ. (Inset) Illustrates the compatibility of the estimated exponents with the finite size decay behavior of the correlations at the largest distance.

$u = U - U_c$ and we series expand the scaling functions f_0^R and f_1^R [76]. Adding corrections to scaling yields series expansion coefficients of f_1^R and values for ω, which vanish within error bars and significantly degrades the quality of the data collapse. This behavior is in accordance with the lack of drift for larger lattices and reduces our scaling ansatz to the first term without scaling corrections. For a fit to the data of systems $L \geq 7$ we obtain the critical coupling $U = 6.759(1)$ and the exponent associated with the correlation length $\nu = 0.977(5)$, which allows us to collapse the data in Fig. 2.

Scaling the squared magnetization as a function of a dimensionless quantity, such as a correlation ratio R_{m^2}, allows us to eliminate the exponent ν from scaling and the FSS ansatz reduces to $m^2(R_{m^2}, L) = L^{1-\eta_\phi} f_0^m(R_{m^2})$, where we assume $z = 1$ [46,76]. Figure 3 shows the fit to the data, where we have expanded $f_0^m(R_{m^2})$ up to second order. We obtain a stable estimate $\eta_\phi = 0.531(1)$; higher expansion orders do not alter the result and corrections to scaling behave similar to the case for ν above. The inset of Fig. 3 shows the compatibility of our estimate with a commonly used approach to extract η_ϕ from the scaling of the magnetization or the spin correlations at the maximum distance $C(r_{\max})$, which decay proportional to $L^{-(1+\eta_\phi)}$ at the critical point. To check the consistency of the extracted exponents, we compute the critical exponent of the order parameter $\beta = (1 + \eta_\phi)\nu/2 = 0.748(4)$ and successfully perform a data collapse of the squared magnetization in Fig. 2. In addition we compare with the data collapse obtained using a Gaussian process regression introduced in Ref. [77]. The regression assumes only the smoothness of the scaling function $m^2(U, L) = L^{-2\beta/\nu} f_0^m[(U - U_c)L^{1/\nu}]$, rather than a specific polynomial form and agrees

within error bars with our estimate $\beta/\nu = 0.766(6)$ (cf., Supplemental Material [72]).

Following the same procedure, we extract the anomalous dimension of the fermions η_ψ from the off-diagonal elements of the single-particle Green's function $G_{ab}(\mathbf{k}) = \langle a_\mathbf{k}^\dagger b_\mathbf{k} \rangle$ with the FSS ansatz $G_{ab}(\mathbf{k}_{\min})(R_{m^2}, L) = L^{-\eta_\psi} f_0^G(R_{m^2})$, where we again assume $z = 1$ [47,76]. At zero momentum, $G_{ab}(\mathbf{0}) = 0$, as $G_{aa}(\mathbf{0}) = G_{bb}(\mathbf{0}) = 1/2$ measures the local density per flavor, such that one has to resort to using the smallest lattice momentum $\mathbf{k}_{\min} = (2\pi/L, 0)$, where $\mathbf{k}_{\min} \to 0$ in the TDL. Here the finite size corrections require us to neglect system sizes $L < 11$ in order to avoid scaling corrections. The fit to the data yields the estimate $\eta_\psi = 0.177(1)$ (cf., Supplemental Material [72]).

The off-diagonal single-particle Green's function is proportional to the quasiparticle weight (residue of the quasiparticle pole) $Z_{\mathbf{k}_{\min}} = 2 G_{ab}(\mathbf{k}_{\min})$ [47,78,79]. As the critical point is approached from the noninteracting limit, growing correlations lead to increasing fluctuations in the semimetal near the Fermi energy and the well-defined fermionic quasiparticle character of the chiral limit $Z_{\mathbf{k}_{\min}} = 1$ is monotonously diminished $Z_{\mathbf{k}_{\min}} \to 0$ as $U \to U_c$ [44,78]. In order to show the consistency of our estimates, we plot the expected behavior of the residue of the quasiparticle pole $Z_{\mathbf{k}_{\min}} \sim (U_c - U)^{\nu \eta_\psi}$ in Fig. 4(b) using the previously extracted exponents (dashed line). Beyond the critical point, the Fermi point surface is gapped out as the single-particle gap $\Delta_{\rm sp} \sim (U - U_c)^{z\nu}$ (not shown), and the fermionic primary excitations are replaced by the Goldstone bosons, which originate from the spontaneous continuous symmetry breaking of the spin rotational symmetry in the TDL.

In addition, we determine the single-particle gap $\Delta_{\rm sp}(\mathbf{k})$ from a fit to the asymptotic long imaginary-time
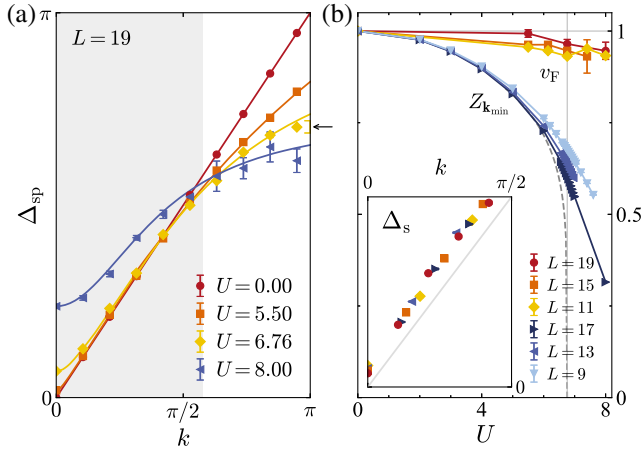
FIG. 4. (a) The single-particle gap along k_x ($k_y = 0$) for different interactions strengths for an $L = 19$ system from which the effective speed of light (equal to the Fermi velocity v_F at $U = 0$) has been extracted from a fit of the relativistic dispersion to the data points. (b) The quasiparticle weight $Z_{k_{\min}}(U)$ and the effective speed of light $v_F(U)$ for different system sizes and the momentum dependence of the spin gap Δ_s (inset).

behavior of the single-particle Green's function $G_{aa}(\mathbf{k}, \tau) = \langle a_{\mathbf{k}}^{\dagger}(\tau) a_{\mathbf{k}}(0) \rangle \propto \exp[-\tau \Delta_{\text{sp}}(\mathbf{k})]$ [80]. In the Supplemental Material [72] we provide evidence for the relativistic finite size scaling $\Delta_{\text{sp}} \sim L^{-z}$ close to criticality, which validates our assumption that $z = 1$. Cross sections of the momentum resolved excitation gap in Fig. 1 are shown for different values of U in Fig. 4(a). The bandwidth decreases significantly with growing U, yet the single-particle excitations close to the boundary of the BZ converge to a finite value at rather high energies, as indicated by the arrow for $U = 6.76$ in the TDL. This implies that no additional zero modes are introduced by correlations [54,56]. In order to study the impact of interactions on the low-energy dispersion, we fit the relativistic single-particle dispersion $\Delta_{\text{sp}}(k) = [\Delta_{\text{sp}}(0)^2 + (v_F(U)k)^2]^{1/2}$ to the data for momenta within the gray shaded region to estimate the Fermi velocity v_F. This approach is validated by the expected spectrum both

in the semimetallic and the symmetry broken phase. Exactly at the quantum critical point the spectrum is more complex [81,82] and the excitation velocity corresponds to the speed of light of the conformal field theory. As illustrated in Fig. 4(b) in the approach of the phase transition from the noninteracting limit the speed of light remains approximately constant. In our case $v_F \approx v_F^0 \approx 1$, which is not necessarily the case in general—the RG scaling ansatz for the quasi-particle residue simply implies $v_F \sim (U_c - U)^{\nu(z-1)}$ to remain regular in the vicinity of the relativistic critical point [44]. Beyond the critical point, the fermionic primary excitations are replaced by their bosonic counterpart such that close to U_c the spin wave velocity $v_\phi \approx v_F$. The inset in Fig. 4(b) illustrates the similar excitation velocities by comparing the momentum dependence of the spin gap $\Delta_s(k) \propto v_\phi k$ with the Fermi velocity v_F^0 [83].

Discussion.—Figure 5 shows our results for the critical exponents in the context of recent results for different numbers of fermion species. For each case we have consistent estimates for the large-N limit from ϵ expansion [17,30] and $1/N$ corrections [48]. The same holds for the limit $N = 0$ where no fermions couple to the bosonic order parameter and high-precision estimates from Monte Carlo simulations and conformal bootstrap calculations exist [84,85]. For relatively small numbers of fermion species, $N \lesssim 16$, estimates from Monte Carlo (MC) simulations [41,46,50] and analytic expansions differ significantly. For the analytical expansion results we include results at fixed expansion order ($\epsilon = 1$) as indicated (lines), the range of values spanned by the Padé approximant with all pole-free combinations of numerator and denominator order from one to the maximum expansion order available (shaded-hatched areas), as well as estimates from functional RG [22,49]. The MC results generally follow the trends set by the analytical predictions, but for η_ϕ in the $1/N$ approximation. While the MC data are scattered, there appears to be a common trend for $\nu, \eta_\phi \lesssim 1$, which roughly follows the ϵ expansion at fixed $O(\epsilon^2)$. The tension between different results from MC simulations could be attributed to the
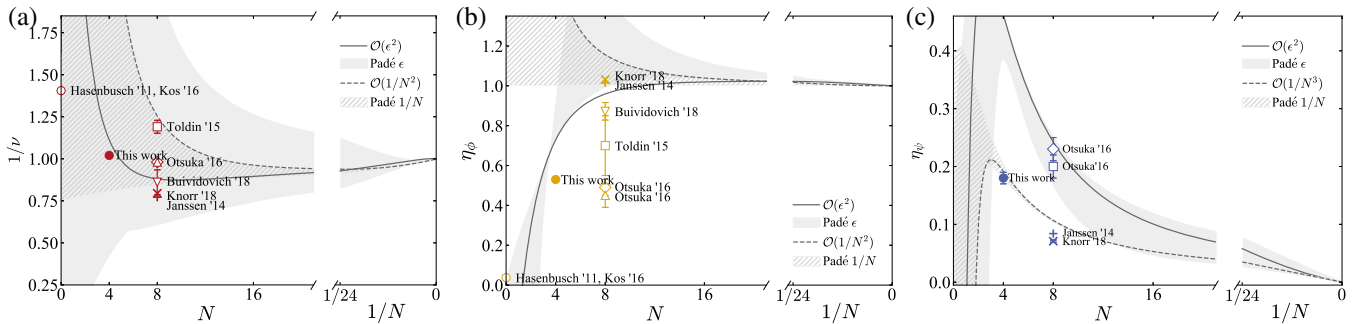

FIG. 5. Chiral Heisenberg GNY universality class. Comparison of estimates for (a) the correlation-length exponent $1/\nu$, (b) the boson anomalous dimension η_ϕ, and (c) the fermion anomalous dimension η_ψ for different numbers of fermion species, from Monte Carlo simulations (filled and open markers) [41,46,50,84], conformal bootstrap [85], and functional RG (+, ×) [22,49], as well as fixed order expansions and Padé approximants for the series from ϵ expansion [17,30] and $1/N$ expansion [48] (lines and shaded areas).

possibility that the lattices' sizes reached so far are simply not within the asymptotic scaling regime. Also, different implementation of lattice fermions may avoid FSS contributions from nonleading irrelevant fields, as has been seen recently in the context of quantum spin models [86]. Most importantly, the different maximum system sizes used limit the momentum resolution of the relativistic dispersion at low energies. This is in contrast to SLAC fermions, which appear to be subject to smaller finite size corrections, which we further quantify for several correlation ratios in the Supplemental Material [72].

Conclusion.—We have presented the first QMC investigation of the critical properties of the $N = 4$ chiral Heisenberg GNY quantum phase transition in $(2 + 1)$D. To account for the ambiguity in the choice of the correlation ratio, fit ranges, and included lattice sizes, we report our conservative estimates for the critical exponents $\nu = 0.98(1)$, $\eta_\phi = 0.53(1)$, and $\eta_\psi = 0.18(1)$. The lattice realization of a single Dirac cone allowed us to significantly reduce finite size effects and access the regime of small fermion species numbers, which is essential to sort out the disparate results from complementary methods. Our approach opens the possibility to simulate the previously unexplored $N = 2$ chiral Ising GNY transition and can be generalized to higher numbers of fermion flavors N_f. The single Dirac cone can be further generalized to anisotropic-, semi-, and birefringent Dirac semimetals [87–90], which we leave to future investigations.

---

[*] thomas.lang@uibk.ac.at

[1] D. J. Gross and A. Neveu, Dynamical symmetry breaking in asymptotically free field theories, Phys. Rev. D **10**, 3235 (1974).

[2] J. Zinn-Justin, Four-fermion interaction near four dimensions, Nucl. Phys. **B367**, 105 (1991).

[3] O. Vafek and A. Vishwanath, Dirac fermions in solids: From high-tc cuprates and graphene to topological insulators and Weyl semimetals, Annu. Rev. Condens. Matter Phys. **5**, 83 (2014).

[4] T. Wehling, A. Black-Schaffer, and A. Balatsky, Dirac materials, Adv. Phys. **63**, 1 (2014).

[5] N. P. Armitage, E. J. Mele, and A. Vishwanath, Weyl and Dirac semimetals in three-dimensional solids, Rev. Mod. Phys. **90**, 015001 (2018).

[6] S. M. Young, S. Zaheer, J. C. Y. Teo, C. L. Kane, E. J. Mele, and A. M. Rappe, Dirac Semimetal in Three Dimensions, Phys. Rev. Lett. **108**, 140405 (2012).

[7] S. M. Young and C. L. Kane, Dirac Semimetals in Two Dimensions, Phys. Rev. Lett. **115**, 126803 (2015).

[8] V. N. Kotov, B. Uchoa, V. M. Pereira, F. Guinea, and A. H. Castro Neto, Electron-electron interactions in graphene: Current status and perspectives, Rev. Mod. Phys. **84**, 1067 (2012).

[9] R. Bistritzer and A. H. MacDonald, Moiré bands in twisted double-layer graphene, Proc. Natl. Acad. Sci. U.S.A. **108**, 12233 (2011).

[10] Y. Cao, J. Y. Luo, V. Fatemi, S. Fang, J. D. Sanchez-Yamagishi, K. Watanabe, T. Taniguchi, E. Kaxiras, and P. Jarillo-Herrero, Superlattice-Induced Insulating States and Valley-Protected Orbits in Twisted Bilayer Graphene, Phys. Rev. Lett. **117**, 116804 (2016).

[11] K. Kim, A. DaSilva, S. Huang, B. Fallahazad, S. Larentis, T. Taniguchi, K. Watanabe, B. J. LeRoy, A. H. MacDonald, and E. Tutuc, Tunable moiré bands and strong correlations in small-twist-angle bilayer graphene, Proc. Natl. Acad. Sci. U.S.A. **114**, 3364 (2017).

[12] Y. Cao, V. Fatemi, A. Demir, S. Fang, S. L. Tomarken, J. Y. Luo, J. D. Sanchez-Yamagishi, K. Watanabe, T. Taniguchi, E. Kaxiras, R. C. Ashoori, and P. Jarillo-Herrero, Correlated insulator behaviour at half-filling in magic-angle graphene superlattices, Nature (London) **556**, 80 (2018).

[13] Y. Cao, V. Fatemi, S. Fang, K. Watanabe, T. Taniguchi, E. Kaxiras, and P. Jarillo-Herrero, Unconventional superconductivity in magic-angle graphene superlattices, Nature (London) **556**, 43 (2018).

[14] M. Yankowitz, S. Chen, H. Polshyn, Y. Zhang, K. Watanabe, T. Taniguchi, D. Graf, A. F. Young, and C. R. Dean, Tuning superconductivity in twisted bilayer graphene, Science **363**, 1059 (2019).

[15] I. F. Herbut, Interactions and Phase Transitions on Graphene's Honeycomb Lattice, Phys. Rev. Lett. **97**, 146401 (2006).

[16] M. Schuler, S. Hesselmann, S. Whitsitt, T. C. Lang, S. Wessel, and A. M. Läuchli, Torus spectroscopy of the Gross-Neveu-Yukawa quantum field theory: Free Dirac versus chiral Ising fixed point, arXiv:1907.05373.

[17] B. Rosenstein, H.-L. Yu, and A. Kovner, Critical exponents of new universality classes, Phys. Lett. B **314**, 381 (1993).

[18] S. Chandrasekharan and A. Li, Quantum critical behavior in three dimensional lattice Gross-Neveu models, Phys. Rev. D **88**, 021701(R) (2013).

[19] S. Hands, Towards critical physics in $2 + 1$d with u(2N)-invariant fermions, J. High Energy Phys. 11 (2016) 015.

[20] S. Hands, A. Kocic, and J. Kogut, Four-fermi theories in fewer than four dimensions, Ann. Phys. (N.Y.) **224**, 29 (1993).

[21] L. Kärkkäinen, R. Lacaze, P. Lacock, and B. Petersson, Critical behaviour of the three-dimensional Gross-Neveu and Higgs-Yukawa models, Nucl. Phys. **B415**, 781 (1994).

[22] L. Janssen and I. F. Herbut, Antiferromagnetic critical point on graphene's honeycomb lattice: A functional renormalization group approach, Phys. Rev. B **89**, 205403 (2014).

[23] L. Wang, P. Corboz, and M. Troyer, Fermionic quantum critical point of spinless fermions on a honeycomb lattice, New J. Phys. **16**, 103008 (2014).

[24] L. Wang, M. Iazzi, P. Corboz, and M. Troyer, Efficient continuous-time quantum Monte Carlo method for the

ground state of correlated fermions, Phys. Rev. B **91,** 235151 (2015).

[25] Z.-X. Li, Y.-F. Jiang, and H. Yao, Fermion-sign-free Majorana-quantum-Monte-Carlo studies of quantum critical phenomena of Dirac fermions in two dimensions, New J. Phys. **17,** 085003 (2015).

[26] Z.-X. Li, Y.-F. Jiang, and H. Yao, Solving the fermion sign problem in quantum Monte Carlo simulations by Majorana representation, Phys. Rev. B **91,** 241117(R) (2015).

[27] S. Hesselmann and S. Wessel, Thermal Ising transitions in the vicinity of two-dimensional quantum critical points, Phys. Rev. B **93,** 155157 (2016).

[28] E. Huffman and S. Chandrasekharan, Fermion bag approach to Hamiltonian lattice field theories in continuous time, Phys. Rev. D **96,** 114502 (2017).

[29] B. Ihrig, L. N. Mihaila, and M. M. Scherer, Critical behavior of Dirac fermions from perturbative renormalization, Phys. Rev. B **98,** 125109 (2009)..

[30] N. Zerf, L. N. Mihaila, P. Marquard, I. F. Herbut, and M. M. Scherer, Four-loop critical exponents for the Gross-Neveu-Yukawa models, Phys. Rev. D **96,** 096010 (2017).

[31] J. E. Drut and T. A. Lähde, Lattice field theory simulations of graphene, Phys. Rev. B **79,** 165425 (2009).

[32] S. Hands and C. Strouthos, Quantum critical behavior in a graphenelike model, Phys. Rev. B **78,** 165423 (2008).

[33] S. Chandrasekharan and A. Li, Fermion Bags, Duality, and the Three Dimensional Massless Lattice Thirring Model, Phys. Rev. Lett. **108,** 140404 (2012).

[34] M. M. Scherer and I. F. Herbut, Gauge-field-assisted Kekulé quantum criticality, Phys. Rev. B **94,** 205136 (2016).

[35] S.-K. Jian and H. Yao, Fermion-induced quantum critical points in two-dimensional Dirac semimetals, Phys. Rev. B **96,** 195162 (2017).

[36] Y.-F. Jiang, Z.-X. Li, S. A. Kivelson, and H. Yao, Charge-4e superconductors: A Majorana quantum Monte Carlo study, Phys. Rev. B **95,** 241103(R) (2017).

[37] Z.-X. Li, Y.-F. Jiang, S.-K. Jian, and H. Yao, Fermion-induced quantum critical points, Nat. Commun. **8,** 314 (2017).

[38] Z.-X. Li, A. Vaezi, C. B. Mendl, and H. Yao, Numerical observation of emergent spacetime supersymmetry at quantum criticality, Sci. Adv. **4,** eaau1463 (2018).

[39] L. Classen, I. F. Herbut, and M. M. Scherer, Fluctuation-induced continuous transition and quantum criticality in Dirac semimetals, Phys. Rev. B **96,** 115132 (2017).

[40] B. H. Wellegehausen, D. Schmidt, and A. Wipf, Critical flavor number of the Thirring model in three dimensions, Phys. Rev. D **96,** 094504 (2017).

[41] Y. Otsuka, K. Seki, S. Sorella, and S. Yunoki, Quantum criticality in the metal-superconductor transition of interacting Dirac fermions on a triangular lattice, Phys. Rev. B **98,** 035126 (2018).

[42] X. Y. Xu, K. T. Law, and P. A. Lee, Kekule valence bond order in an extended Hubbard model on the honeycomb lattice, with possible applications to twisted bilayer graphene, Phys. Rev. B **98,** 121406 (2018).

[43] E. Torres, L. Classen, I. F. Herbut, and M. M. Scherer, Fermion-induced quantum criticality with two length scales in Dirac systems, Phys. Rev. B **97,** 125137 (2018).

[44] I. F. Herbut, V. Juričić, and B. Roy, Theory of interacting electrons on the honeycomb lattice, Phys. Rev. B **79,** 085116 (2009).

[45] F. F. Assaad and I. F. Herbut, Pinning the Order: The Nature of Quantum Criticality in the Hubbard Model on Honeycomb Lattice, Phys. Rev. X **3,** 031010 (2013).

[46] F. Parisen Toldin, M. Hohenadler, F. F. Assaad, and I. F. Herbut, Fermionic quantum criticality in honeycomb and π-flux Hubbard models: Finite-size scaling of renormalization-group-invariant observables from quantum Monte Carlo, Phys. Rev. B **91,** 165108 (2015).

[47] Y. Otsuka, S. Yunoki, and S. Sorella, Universal Quantum Criticality in the Metal-Insulator Transition of Two-Dimensional Interacting Dirac Electrons, Phys. Rev. X **6,** 011029 (2016).

[48] J. A. Gracey, Large n critical exponents for the chiral Heisenberg Gross-Neveu universality class, Phys. Rev. D **97,** 105009 (2018).

[49] B. Knorr, Critical chiral Heisenberg model with the functional renormalization group, Phys. Rev. B **97,** 075129 (2018).

[50] P. Buividovich, D. Smith, M. Ulybyshev, and L. von Smekal, Hybrid-Monte-Carlo study of competing order in the extended fermionic Hubbard model on the hexagonal lattice, Phys. Rev. B **98,** 235129 (2018).

[51] Z. H. Liu, X. Y. Xu, Y. Qi, K. Sun, and Z. Y. Meng, Elective-momentum ultrasize quantum Monte Carlo method, Phys. Rev. B **99,** 085114 (2019).

[52] L. Susskind, Lattice fermions, Phys. Rev. D **16,** 3031 (1977).

[53] K. G. Wilson, *New Phenomena in Subnuclear Physics* (Springer, New York, 1977), Chap. 6, p. 69142.

[54] P. Nason, The lattice Schwinger model with SLAC fermions, Nucl. Phys. **B260,** 269 (1985).

[55] S. Chandrasekharan and U.-J. Wiese, An introduction to chiral symmetry on the lattice, Prog. Part. Nucl. Phys. **53,** 373 (2004).

[56] C. Gattringer and C. B. Lang, *Quantum Chromodynamics on the Lattice*, Lecture Notes in Physics Vol. 788 (Springer, Berlin, 2010).

[57] S. D. Drell, M. Weinstein, and S. Yankielowicz, Strong-coupling field theories. ii. Fermions and gauge fields on a lattice, Phys. Rev. D **14,** 1627 (1976).

[58] L. H. Karsten and J. Smit, The vacuum polarization with SLAC lattice fermions, Phys. Lett. **85B,** 100 (1979).

[59] A. Kirchberg, J. D. Länge, and A. Wipf, From the Dirac operator to Wess-Zumino models on spatial lattices, Ann. Phys. (Amsterdam) **316,** 357 (2005).

[60] G. Bergner, T. Kaestner, S. Uhlmann, and A. Wipf, Low-dimensional supersymmetric lattice models, Ann. Phys. (Amsterdam) **323,** 946 (2008).

[61] T. Kästner, G. Bergner, S. Uhlmann, A. Wipf, and C. Wozar, Two-dimensional Wess-Zumino models at intermediate couplings, Phys. Rev. D **78,** 095001 (2008).

[62] G. Bergner, Complete supersymmetry on the lattice and a no-go theorem, J. High Energy Phys. 01 (2010) 024.

[63] R. Flore, D. Körner, A. Wipf, and C. Wozar, Supersymmetric nonlinear o(3) sigma model on the lattice, J. High Energy Phys. 11 (2012) 159.

[64] H. Nielsen and M. Ninomiya, Absence of neutrinos on a lattice: (i). Proof by homotopy theory, Nucl. Phys. **B185**, 20 (1981).

[65] H. Nielsen and M. Ninomiya, Absence of neutrinos on a lattice: (ii). Intuitive topological proof, Nucl. Phys. **B193**, 173 (1981).

[66] H. Nielsen and M. Ninomiya, A no-go theorem for regularizing chiral fermions, Phys. Lett. **105B**, 219 (1981).

[67] R. G. Campos and E. S. Tututi, Ultralocality on the lattice, arXiv:hep-lat/0208053.

[68] G. Sugiyama and S. Koonin, Auxiliary field Monte-Carlo for quantum many-body ground states, Ann. Phys. (N.Y.) **168**, 1 (1986).

[69] F. Assaad and H. Evertz, World-line and Determinantal Quantum Monte Carlo Methods for Spins, Phonons and Electrons, in *Computational Many-Particle Physics*, edited by H. Fehske, R. Schneider, and A. Weiße (Springer, Berlin, 2008), pp. 277–356.

[70] Z.-X. Li, Y.-F. Jiang, and H. Yao, Majorana-Time-Reversal Symmetries: A Fundamental Principle for Sign-Problem-Free Quantum Monte Carlo Simulations, Phys. Rev. Lett. **117**, 267002 (2016).

[71] Z.-C. Wei, Semigroup approach to the sign problem in quantum Monte Carlo simulations, arXiv:1712.09412.

[72] See Supplemental Material at http://link.aps.org/supplemental/10.1103/PhysRevLett.123.137602 for additional information on the finite size scaling analysis of the critical exponents and simulation details, which includes Ref. [73].

[73] R. Winkler and U. Zülicke, Discrete symmetries of low-dimensional Dirac models: A selective review with a focus on condensed-matter realizations, ANZIAM J. **57**, 3 (2015).

[74] R. K. Kaul, Spin Nematics, Valence-Bond Solids, and Spin Liquids in SO(n) Quantum Spin Models on the Triangular Lattice, Phys. Rev. Lett. **115**, 157202 (2015).

[75] S. Pujari, T. C. Lang, G. Murthy, and R. K. Kaul, Interaction-Induced Dirac Fermions from Quadratic Band Touching in Bilayer Graphene, Phys. Rev. Lett. **117**, 086404 (2016).

[76] M. Campostrini, A. Pelissetto, and E. Vicari, Finite-size scaling at quantum transitions, Phys. Rev. B **89**, 094516 (2014).

[77] K. Harada, Bayesian inference in the scaling analysis of critical phenomena, Phys. Rev. E **84**, 056704 (2011).

[78] W. F. Brinkman and T. M. Rice, Application of Gutzwiller's variational method to the metal-insulator transition, Phys. Rev. B **2**, 4302 (1970).

[79] E. Fradkin, *Field Theories of Condensed Matter Physics* (Cambridge University Press, Cambridge, England, 2013).

[80] M. Feldbacher and F. F. Assaad, Efficient calculation of imaginary-time-displaced correlation functions in the projector auxiliary-field quantum Monte Carlo algorithm, Phys. Rev. B **63**, 073105 (2001).

[81] M. Schuler, S. Whitsitt, L.-P. Henry, S. Sachdev, and A. M. Läuchli, Universal Signatures of Quantum Critical Points from Finite-Size Torus Spectra: A Window into the Operator Content of Higher-Dimensional Conformal Field Theories, Phys. Rev. Lett. **117**, 210401 (2016).

[82] A. Sen, H. Suwa, and A. W. Sandvik, Velocity of excitations in ordered, disordered, and critical antiferromagnets, Phys. Rev. B **92**, 195145 (2015).

[83] B. Roy, V. Juričić, and I. F. Herbut, Emergent Lorentz symmetry near fermionic quantum critical points in two and three dimensions, J. High Energy Phys. 16 (2016) 18.

[84] M. Hasenbusch and E. Vicari, Anisotropic perturbations in three-dimensional o(n)-symmetric vector models, Phys. Rev. B **84**, 125136 (2011).

[85] F. Kos, D. Poland, D. Simmons-Duffin, and A. Vichi, Precision islands in the Ising and o(n) models, J. High Energy Phys. 16 (2016) 36.

[86] N. Ma, P. Weinberg, H. Shao, W. Guo, D.-X. Yao, and A. W. Sandvik, Anomalous Quantum-Critical Scaling Corrections in Two-Dimensional Antiferromagnets, Phys. Rev. Lett. **121**, 117202 (2018).

[87] B. Roy and M. S. Foster, Quantum Multicriticality near the Dirac-Semimetal to Band-Insulator Critical Point in Two Dimensions: A Controlled Ascent from One Dimension, Phys. Rev. X **8**, 011049 (2018).

[88] M. P. Kennett, N. Komeilizadeh, K. Kaveh, and P. M. Smith, Birefringent breakup of Dirac fermions on a square optical lattice, Phys. Rev. A **83**, 053636 (2011).

[89] H. Watanabe, Y. Hatsugai, and H. Aoki, Manipulation of the Dirac cones and the anomaly in the graphene related quantum hall effect, J. Phys. Conf. Ser. **334**, 012044 (2011).

[90] B. Roy, M. P. Kennett, K. Yang, and V. Juričić, From Birefringent Electrons to a Marginal or Non-Fermi Liquid of Relativistic Spin-1/2 Fermions: An Emergent Superuniversality, Phys. Rev. Lett. **121**, 157602 (2018).